Efficient and directional excitation of surface plasmon polaritons by oblique incidence on metallic ridges

EDUARDO PISANO,[1,*] CESAR E. GARCIA-ORTIZ,[2] FABIOLA ARMENTA-MONZON,[3] MANUEL GARCIA-MENDEZ,[3] AND VICTOR COELLO[1]

[1]*CICESE, Unidad Monterrey, Alianza Centro 504, Apodaca, NL, 66629, Mexico*
[2]*CONACYT – CICESE, Unidad Monterrey, Alianza Centro 504, PIIT Apodaca, 66629, Mexico*
[3]*CICFIM, FCFM–UANL, Manuel L. Barragán S/N, Cd. Universitaria, N.L., 66450, Mexico*
**episano@cicese.edu.mx*

Abstract: For many years, the search for efficient surface plasmon polariton (SPP) excitation mechanisms has been a recurring matter in the development of compact plasmonic devices. In this work, we excited SPPs illuminating a subwavelength metallic ridge with a focused spot to characterize the coupling efficiency by varying the incidence angle of the excitation beam from –50° to 50°. The intensity distribution of the excited SPPs was measured using leakage radiation microscopy to determine the relative coupling efficiency in the wavelength interval from 740–840 nm. We modeled the excitation efficiency as a function of the incidence angle using a simple analytical diffraction model. Two ridges of different width (200 and 500 nm) were used to compare results and validate the model. The experimental results show a higher coupling efficiency at oblique incidence, where the coupling was enhanced by factors of 2x for the 500-nm-wide ridge, and 3x for the 200-nm-wide ridge, as well as unidirectional SPP excitation. The experimental results are in good agreement with the proposed model.

OCIS codes: (240.6680) Surface plasmons; (100.0100) Image processing; (260.0260) Physical optics.

References and links

1. E. Kretschmann and H. Raether, "Radiative decay of non-radiative surface plasmons excited by light," Zeitschrift für Physik **23**(12), 2135–2136 (1968).
2. I. P. Radko, S. I. Bozhevolnyi, G. Brucoli, L. Martín-Moreno, F. J. García-Vidal, and A. Boltasseva, "Efficiency of local surface plasmon polariton excitation on ridges," Phys. Rev. B **78**(11), 115115 (2008).
3. M.-D. He, J.-Q. Liu, Z.-Q. Gong, S. Li, Y.-F. Luo, "Directional excitation of surface plasmon polaritons in structure of subwavelength metallic holes," Opt. Comm. **285**(2), 182–185 (2012).
4. I. Radko, A. Evlyukhin, A. Boltasseva, and S. Bozhevolnyi, "Refracting surface plasmon polaritons with nanoparticle arrays," Opt. Express **16**(6), 3924–3930 (2008).
5. E. Pisano, V. Coello, C. E. Garcia-Ortiz, Y. Chen, J. Beerman and S.I. Bozhevolnyi, "Plasmonic channel waveguides in random arrays of metallic nanoparticles," Opt. Express **24**(15), 17080-17089 (2016).
6. T. Xu, Y. Zhao, D. Gan, C. Wang, C. Du, and X. Luo, "Directional excitation of surface plasmons with subwavelength slits," Appl. Phys. Lett. **92**(10), 101501 (2008).
7. C. L. C. Smith, A. H. Thilsted, C. E. Garcia-Ortiz, I. P. Radko, R. Marie, C. Jeppesen, C. Vannahme, S. I. Bozhevolnyi, and A. Kristensen, "Efficient excitation of channel plasmons in tailored, UV-lithography-defined V-grooves," Nano Lett. **14**(3), 1659–1664 (2014).
8. Z. Han, C. E. Garcia-Ortiz, I. P. Radko, and S. I. Bozhevolnyi, "Detuned-resonator induced transparency in dielectric-loaded plasmonic waveguides," Opt. Express **38**(6), 875–877 (2013).
9. H. Ditlbacher, J. R. Krenn, G. Schider, A. Leitner, and F. R. Aussenegg, "Two-dimensional optics with surface plasmon polaritons," Appl. Phys. **81**(10), 1762–1764 (2002).
10. A. Klick, S. de la Cruz, C. Lemke, M. Großmann, H. Beyer, J. Fiutowski, H.-G. Rubahn, E. R. Méndez, and M. Bauer, "Amplitude and phase of surface plasmon polaritons excited at a step edge," Appl. Phys. B-Lasers O. **122**(4), 79 (2016).
11. C.E. Garcia-Ortiz, E. Pisano and V. Coello, "Description and characterization of plasmonic Gaussian beams," J. Opt. **19**(8), 085001 (2017).
12. A. Drezet, A. Stepanov, A. Hohenau, B. Steinberger, N. Galler, H. Ditlbacher, A. Leitner, F. Aussenegg, J. Krenn, M. Gonzalez, and J. C. Weeber, "Surface plasmon interference fringes in back-reflection," Europhysics Lett. **74**(4), 693–698 (2006).

13. H. Liu, P. Lalanne, X. Yang, and J. P. Hugonin, "Surface plasmon generation by subwavelength isolated objects," IEEE J. Sel. Top. Quantum Electron. **14**(6), 1522–1529 (2008).
14. H. Kim and B. Lee, "Unidirectional surface plasmon polariton excitation on single slit with oblique backside illumination," Plasmonics **4**(6), 153–159 (2009).
15. H. Hu, X. Zeng, Y. Zhao, J. Li, H. Song, G. Song, Y. Xu and Q. Gan, "Unidirectional coupling of surface plasmon polaritons by a single slit on a metal substrate," IEEE Photon. Technol. Lett. **28**(21), 2395–2398 (2016).
16. Y. Sonnefraud, S. Kerman, G. D. Martino, D. Y. Lei and S. A. Maier, "Directional excitation of surface plasmon polaritons via nanoslits under varied incidence observed using leakage radiation microscopy," Opt. Express **20**(5), 4893–4902 (2012).
17. C. Vieu, F. Carcenac, A. Pepin, Y. Chen, M. Mejias, A. Lebib, L. Manin-Ferlazzo, L. Couraud, and H. Launois, "Electron beam lithography: resolution limits and applications," Appl. Surf. Sci. **164**(1-4), 111–117 (2000).
18. A. Drezet, A. Hohenau, D. Koller, A. Stepanov, H. Ditlbacher, B. Steinberger, F. R. Aussenegg, A. Leitner, and J. R. Krenn, "Leakage radiation microscopy of surface plasmon polaritons," Mater. Sci. Eng. B **149**(3), 220–229 (2008).
19. K. Hassan, A. Bouhelier, T. Bernardin, G. Colas-des-Francs, J. C. Weeber, A. Dereux, and R. Espiau de Lamaestre, "Momentum-space spectroscopy for advanced analysis of dielectric-loaded surface plasmon polariton coupled and bent waveguides," Phys. Rev. B **87**(19), 195428 (2013).
20. Y. Z. Umul, "Babinet's principle in the Fraunhofer diffraction by a finite thin wire," Optik **122**(16), 1434–1436 (2011).
21. P. B. Johnson and R. W. Christy, "Optical constants of the noble metals," Phys. Rev. B **6**(12), 4370–4379 (1972).

1. Introduction

Surface plasmon polaritons (SPPs) are evanescent waves which require the use of coupling elements to be excited, such as prisms [1] or diffraction gratings [2], to compensate for the momentum mismatch between photons and SPPs. These two mechanisms are known for (almost) completely coupling the incident light to SPPs. However, in practice, they tend to be too large to be included in integrated devices at the nanometer scale. An alternative, is the use of simpler subwavelength structures patterned on a metal surface. In this context, some proposed geometries that have been investigated for SPP excitation include arrangements of holes [3], single ridges [4, 5], slits [6], micrometric mirrors [7], and refractive-index steps [8], among others [9, 10]. Metallic ridges are of particular interest for its relatively simple geometry and due to its capacity to couple SPPs in a broad wavelength interval, in contrast to gratings which couple efficiently only for the designed wavelength and have a much smaller footprint. SPP beams can be coupled using metallic ridges by tightly focusing light on the structure, e.g. with a microscope objective, to generate two counter-propagating plasmonic beams. Plasmonic Gaussian beams can be generated in this way if the ridge is illuminated with focused Gaussian beam from a laser [11]. This simple nanostructure has been successfully used in a wide variety of applications to excite SPPs and study their interaction with other nanostructured elements [4, 5, 12]. According to theoretical predictions for ridges and slits, the efficiency of the local excitation of SPPs can be improved under oblique illumination [13] and even unidirectional coupling of SPPs can be obtained [14, 15]. However, in practice, the great majority only use the normal incidence of light and less attention has been paid to an oblique illumination of the coupling structures for SPP excitation. The reasons fall mainly in experimental difficulties. Recent experimental work has overcome these issues using a leakage radiation microscopy (LRM) setup that is configured to allow oblique illumination [16]. They demonstrated partially the aforementioned effects of oblique illumination using arrangements of nano-slits for a single wavelength in the visible, nevertheless, the main shortcoming of the work yields in their limited angular spectrum measurements (–20° to 20°), which cuts out important features of the effects.

In this work, we excited SPPs by illuminating single metallic ridges and varying the incidence angle of the excitation beam from –50° to 50°, using a similar LRM setup as reported in reference [15]. Two metallic ridge structures of different widths were characterized in the wavelength interval from 740 to 840 nm, in order to obtain the relative (to normal incidence) coupling efficiencies of the excited SPPs. The two counter-propagating SPPs beams were studied separately and compared with each other. For the theoretical analysis and comparison

with the experimental results, a simple diffraction-based model is presented [14, 16]. The experimental results show that the SPPs excited at oblique incidence present efficient unidirectional propagation and a higher relative coupling efficiency, where the coupling is enhanced by factors of 2x and 3x, for the different ridges.

2. Materials and methods

The sample consisted of a 70-nm-thick gold thin film deposited over a silica substrate, over which the gold ridges were patterned and fabricated with a standard process of electron beam lithography (EBL) [17]. Two gold ridges of same height (h_r = 70 nm) and different widths (w_r = 200 and 500 nm) were fabricated [Fig. 1(a)]. The analysis of the coupling efficiency was performed using LRM image analysis [18, 19]. The LRM setup was modified with the inclusion of a mirror, mounted on a translation stage previous to the focusing objective (100x, NA 0.9), dedicated to steer the trajectory of the incident laser beam to enter through the rear aperture of the objective at different positions with respect to its main axis [Fig. 1(b)]. This arrangement allows to control the angle at which the light leaves the focusing objective, and thereby control the incidence angle θ_i of the beam relative to the perpendicular direction of the sample surface. This process is performed by changing the displacement d_x of the reflected beam along the transverse direction to the optical axis [Fig. 1(b)].

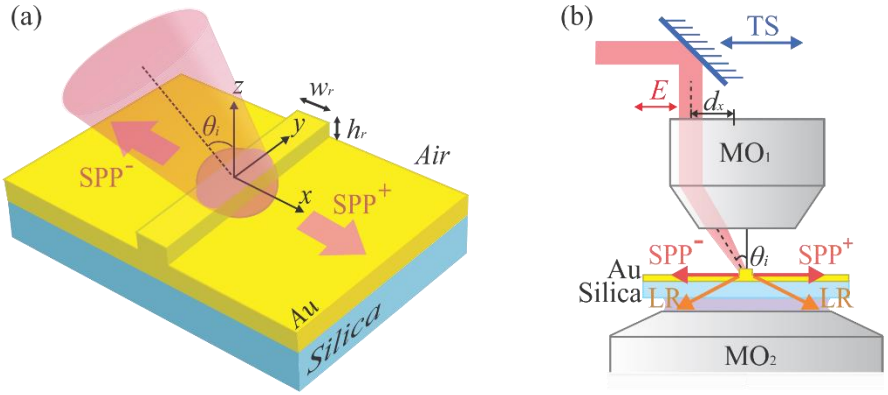

Fig. 1. (a) Schematic of the sample showing the metallic ridge used to couple light into SPPs on top of a gold thin film deposited over a silica substrate. The structure is illuminated with different incidence angles θ_i in the *xz*-plane (perpendicular to the ridge axis *y*). The red arrows corresponds to the counter-propagating SPP beams (SPP^- and SPP^+). (b) Schematic of the central part of the experimental setup. The mirror on the translation stage (TS) is displaced a distance d_x to change the incidence angle of the beam. The leakage radiation (LR) of the excited SPPs is further collected with the immersion objective MO_2.

The laser beam width was previously reduced using a lens of long focal length (1 m), focusing at the rear aperture of the objective, with a beam width of ~35 μm. The reduction of the spot is needed in order to improve the angular resolution of the experiments, as the diameter of the rear aperture of the 100x focusing objective used for this experiment corresponds to only 4 mm. The relation between d_x and θ_i can be obtained by characterizing the displacement of the spot in the Fourier plane (FP) of the LRM setup, i.e. associating spatial displacements to normalized frequency units. The image in the FP can be visualized in a normalized frequency map with coordinate system κ_x–κ_y, where $\kappa_x = k_x/k_0$, and $k_0 = 2\pi/\lambda_0$ is the free-space wave vector of the incident light. The Fourier plane (FP) of the LRM setup was used to calibrate the measurement system.

Two scale factors were needed to completely characterize the system: (1) a scale factor F_1 was used to relate the pixels of the camera with the normalized frequency units, and (2) a scale factor F_2 to relate the displacement of the beam spot with the displacement in pixels of the camera. The process to find the first scale factor was as follows. First, the rear aperture of the

focusing objective was completely illuminated using a beam expander, resulting in the appearance of a bright disk in the FP, which was recorded with a charge-coupled device (CCD) camera [Fig. 2(a)]. The radius of the disc corresponds to the numerical aperture (NA) of the focusing objective (NA = 0.9). The numerical aperture of an objective gives information of its total angular acceptance μ, and is given by NA = n sin(μ), where n is the refractive index of the medium between the sample and the objective (n = 1, in this case). The radius of the disc in pixels R_{px} was measured from the CCD camera to assign the scale factor F_1 = (NA)/R_{px} = 0.90/470 ≈ 0.00191 [Fig. 2(a)]. The process for obtaining the second scale factor was similar. The translation stage was manipulated manually with a micrometer drive which controls the displacement d_x of the beam. The stage was displaced until the illumination spot appeared close to the boundary of the allowed light disc (NA), taking care that the complete spot was visible. The reading in the micrometer at this point showed a displacement d_m = 1.375 mm, which corresponds to a lateral displacement of d_{px} = 402 pixels, relative to the FP origin (defined as the centroid of the NA disc). These results were used to find the second scale factor $F_2 = d_{px}/d_m$ ≈ 292.36 [Fig. 2(c)]. Having both scale factors, and taking into account that $\kappa_x = \sin(\theta_i)$, it was possible to define an expression that relates d_x and θ_i for this experiment as $\theta_i = \arcsin[(F_1F_2)d_x]$.

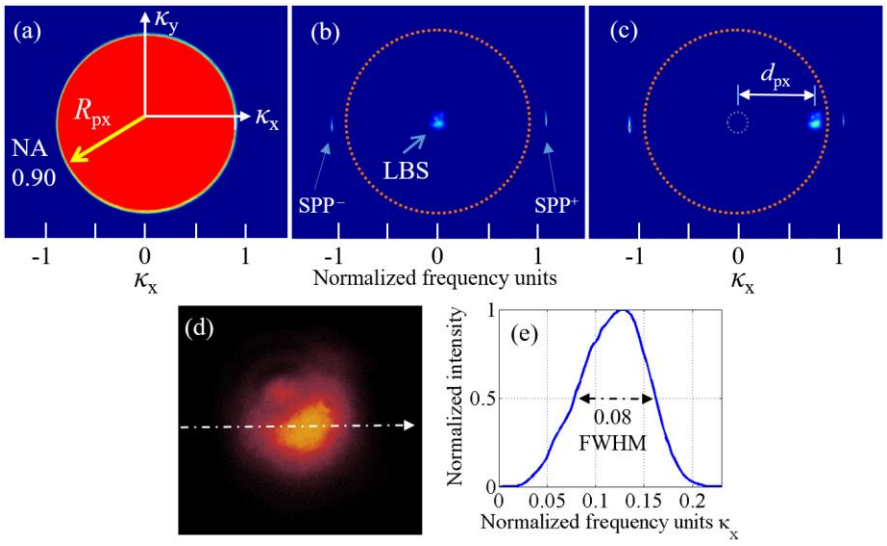

Fig. 2. (a) LRM image of the FP when the rear aperture of the focusing objective is completely illuminated. The bright disc corresponds to the numerical aperture NA = 0.90 of the objective. (b)–(c) LRM images of the FP with the reduced (focused) laser beam spot (LBS), illuminating the ridge at (b) normal and (c) oblique incidence (θ_i = 50°). The spot is displaced a distance d_{px} in pixels from the origin of the FP, that is associated to a change of θ_i. (d) Amplified image of the LBS shown in (b). (e) Transverse intensity cross-section of the LBS in (d). The FWHM = 0.08 of the spot contributes to an angular resolution of ~ 4.5°.

The full-width at half-maximum (FWHM = 0.08) of the laser beam spot at the FP was measured to calibrate the angular resolution of our system, giving a value of $\Delta\theta$ = 4.5°. [Fig. 2(d)–(e)]. The maximum displacement of the micrometer drive (1.375 mm) also gives the maximum angles for oblique illumination, resulting in θ_{max} = ±50.3°, and the number (and size) of displacement steps was defined by dividing the maximum angular spectrum by the angular resolution, giving 11 steps of 125 μm, for each direction.

3. Analytical model

The excitation efficiency of SPPs was estimated by implementing a simple semi-analytical model. The basis of this model considers the excitation of SPPs by coupling to one of the broad range of wave vectors generated by the diffraction caused by illuminating a subwavelength

surface feature. Furthermore, it is assumed that the intensity of the excited SPPs is proportional to the intensity of the diffracted component that matches the SPPs wave vector. The wave-vector spectrum of the diffracted light was calculated from the Fourier transform of the incident field. The formulation for the diffraction of subwavelength structures has been reported before [14, 16], for the case of SPP generation by oblique incidence using nano-slits. An adaptation of such model was implemented for our analysis with a single metallic ridge, where taking advantage of Babinet's principle [20], the field at the ridge for oblique incidence is considered to be

$$E(\mathrm{x}) = \exp\left[i\left(2\pi x \frac{\sin\theta_i}{\lambda_0} \right) \right] \times \mathrm{rect}\left(x \right) \ , \tag{1}$$

where λ_0 is the illumination wavelength. The geometry of the ridge is represented by the rectangle function in Eq. (1), and it is defined as

$$\mathrm{rect}\left(x \right) = \begin{cases} 1 & \text{for} \quad |x| \le \dfrac{w_\mathrm{r}}{2} \\ 0 & \text{elsewhere} \end{cases} \ . \tag{2}$$

The Fourier transform of Eq. (1) gives the field amplitude for every wave vector κ, at any incidence angle, and it is given by

$$\tilde{E}(\kappa) = w_\mathrm{r} \cdot \mathrm{sinc}\left[w_\mathrm{r} \cdot \left(\kappa - \frac{\sin\theta_i}{\lambda_0} \right) \right] . \tag{3}$$

Using this distribution, one can calculate the amplitude and intensity for a given SPP wave vector β and θ_i. For this, we rewrite Eq. (3) to obtain

$$I(\theta_i) = \left| \tilde{E}\left(\beta \right) \right|^2 = \left| w_\mathrm{r} \cdot \mathrm{sinc}\left[w_\mathrm{r} \cdot \left(\beta - \frac{\sin\theta_i}{\lambda_0} \right) \right] \right|^2 . \tag{4}$$

The SPPs excited with the ridge couple to two counter-propagating beams, normal to the direction of the ridge. Each plasmonic beam can be approached individually, and considering each direction as the (+) and (–) direction, we will refer to them using the notation SPP^+ and SPP^-. The intensity of each beam can be obtained by $I^+ = \left| \tilde{E}\left(\beta \right) \right|^2$ and $I^- = \left| \tilde{E}\left(-\beta \right) \right|^2$. Finally, to estimate the relative (to normal incidence) coupling efficiency η_R for a given incidence angle, we simply normalize to get $\eta_\mathrm{R}(\theta_i) = I(\theta_i)/I(0)$. Since the thickness of the gold thin film was set to be 70 nm, the dispersion relation is almost identical to the dispersion of SPPs in a single gold/air interface [18], which is given by

$$\beta = k_0 \sqrt{\frac{\varepsilon_\mathrm{Au}}{\varepsilon_\mathrm{Au} + 1}} \ , \tag{5}$$

where ε_Au is the dielectric function of gold. The values of ε_Au were consulted from [21].

4. Results and Discussion

The measurement of the relative coupling efficiency was performed by capturing images of the image plane of the microscope with a CCD camera. When the ridge was illuminated with the

focused light of the laser (tunable Ti:Sapphire), it was possible to observe in the camera two counter-propagating plasmonic beams [Fig. 3]. A beam blocker (Fourier spatial filter) was used to stop the directly transmitted light (non-coupled light) and avoid the unnecessary saturation of the image. The intensity of each plasmonic beam was calculated via a post-processing image analysis method that consists in integrating the intensity values of the pixels of the camera for a delimited area that covers most of the intensity distribution of the beam [Fig. 3(a)]. Both counter-propagating beams (SPP^+ and SPP^-) are analyzed and measured separately. This process was performed for the whole angular spectrum of incidence angles that our system allowed (–50° to 50°) and for three different wavelengths (740, 790 and 840 nm) [Fig. 4].

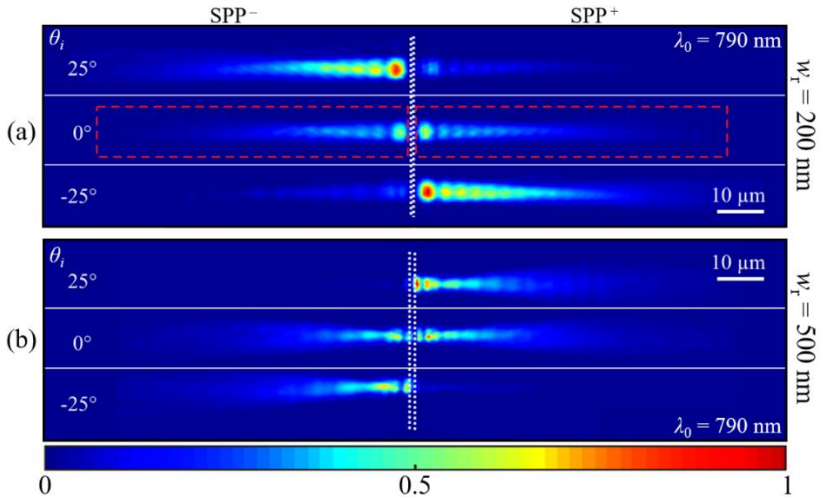

Fig. 3. LRM images of the intensity distribution of SPPs excited at different angles of incidence with θ_i = 25°, 0° and –25°, for the two rectangular ridges (a) w_r = 200 nm and (b) w_r = 500 nm. The wavelength of excitation light was 790 nm. The dotted white lines represent the position of the ridge, while the red dashed rectangles denote the integration area used to calculate the intensity of the beam.

The relative coupling efficiency was simply calculated by normalizing the obtained intensity values with the ones measured at normal incidence (θ_i = 0°). SPPs excited at normal incidence result in a symmetric intensity distribution of the two beams, but for $\theta_i \neq 0°$, we observe notable differences between the SPP^+ and SPP^- beams. The same occurs as the width of the ridge is modified. The variation of θ_i and/or w_r produces a rupture of the symmetry in the field distribution of the diffracted light, thus modifying the efficiency of the SPPs coupled in each direction. One of the most interesting and important results corresponds to the suppression of one of the beams, causing unidirectional excitation of SPPs. This effect can be observed for both ridges, but at different incidence angles. The 200-nm-wide ridge shows a complete extinction of one of the beams around ±50°, while for the 500-nm-wide ridge occurs around ±25° [Fig. 4]. Another effect corresponds to an increase of the relative efficiency at oblique incidence. The relative coupling efficiency was enhanced by factors of ~2x for the 500-nm-wide ridge, and ~3x for the 200-nm-wide ridge. Slight changes can be appreciated as the wavelength was modified (740–840 nm), manifested in small variations (~ 25%) of the relative coupling efficiency, but not as significant or sensitive as for the variations in θ_i or w_r. The described analytical model shows a good agreement with the measurements, as can be appreciated in the semi-analytical fits plotted in Fig. 4. Due to the high sensitivity that small variations of w_r has on the amplitude of the diffracted field (for a given β), was necessary to add a fitting parameter δw_r to account for the small deviations caused in the fabrication of the ridge.

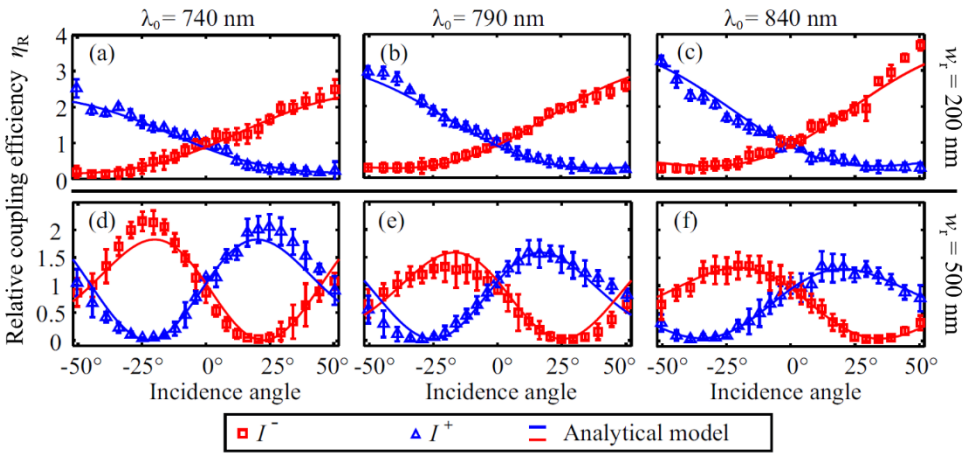

Fig. 4. Experimental measurements of the relative coupling efficiency as a function of the incidence angle for beams propagating to the SPP^- (red squares) and SPP^+ (blue triangles) directions. (a)–(c) correspond to the beams generated with the ridge of width w_r = 200 nm, and (d)–(f) to the ridge of width w_r = 500 nm. The analysis was performed for three different excitation wavelengths λ_0 = 740, 790 and 840 nm. The results are fitted to a semi-analytical model (solid lines).

The numerical fitting process was performed for the three different wavelengths and for the two values of w_r. To prove the validity and accuracy of the method, we calculated the standard deviation of the six obtained values of δw_r, giving a relatively small deviation of 36 nm, which is almost in the limit of resolution of the EBL system used to fabricate these samples. According to the theoretical model presented here, the distribution and directionality of the coupling is solely caused by the amplitudes of the diffraction pattern at the given points $\pm\beta$, indicating that this effect is not caused by interference of the SPP^+ and SPP^- beams, as is the case described in Ref. [6]. Moreover, for the 500-nm-wide ridge, the periodic features of the squared sinc function can be clearly observed in the relative efficiency thanks to the wide angular spectrum of the measurements, i.e. we can identify the relative maximums and minimums of the efficiency function $\eta_R(\theta_i)$ [Fig. 4(d–f)]. The latter cannot be observed, for example in the work in Ref. [16], where the angular measurements were restricted to ±20°.

5. Conclusion

In conclusion, we have studied the coupling efficiency of surface plasmon polaritons excited with metallic single ridges under oblique incidence. We report a clear evidence of coupling enhancements by factors of 2x and 3x for the ridges of different widths, and unidirectional SPP beam excitation. The results and methodology exposed in this work demonstrate an accessible option to attain a wide angular spectrum for oblique-incidence illumination, using microscope objectives of high numerical aperture, and a theoretical approach that allows to predict and tailor the desired behavior of the excited plasmonic beams. Moreover, the coupling efficiency and the propagation direction can be completely controlled by making changes in the incidence angle, without the need to modify the geometry (width) of the ridges. The latter is impractical for experiments that require a single coupling element aside of a plasmonic structure or device. The simplicity of this technique makes it a plausible option for the design and development of new compact plasmonic devices with higher efficiency and control.

Acknowledgments

V.C. and C.E.G.-O. acknowledge the financial support from CONACYT Basic Scientific Research Grants No. 50719 and No. 252621.